NEUROSCIENCE

Shape perception via a high-channel-count neuroprosthesis in monkey visual cortex

Xing Chen[1]*, Feng Wang[1], Eduardo Fernandez[2], Pieter R. Roelfsema[1,3,4]*

Blindness affects 40 million people across the world. A neuroprosthesis could one day restore functional vision in the blind. We implanted a 1024-channel prosthesis in areas V1 and V4 of the visual cortex of monkeys and used electrical stimulation to elicit percepts of dots of light (called phosphenes) on hundreds of electrodes, the locations of which matched the receptive fields of the stimulated neurons. Activity in area V4 predicted phosphene percepts that were elicited in V1. We simultaneously stimulated multiple electrodes to impose visible patterns composed of a number of phosphenes. The monkeys immediately recognized them as simple shapes, motions, or letters. These results demonstrate the potential of electrical stimulation to restore functional, life-enhancing vision in the blind.

Electrical stimulation of the visual cortex has long been proposed as an approach to restore vision in blind people, bypassing severe retinal degeneration or damage to the eye or the optic nerve. Experiments in humans (*1*–*10*) and animals (*11*–*20*) have shown that electrical stimulation of visual cortex can reliably evoke the perception of a dot of light, known as a phosphene. The phosphenes elicited in the primary visual cortex are typically perceived as white or gray dots, although they are occasionally colored (*2*–*4*, *8*), and range in size from a pinpoint to about 2 cm in diameter at arm's length. Subjects perceive phosphenes at the location of the receptive field of the stimulated neurons (*9*, *10*, *17*, *20*). Notably, phosphenes induced in blind but previously sighted subjects are comparable to those in normally sighted subjects, even after decades without sight (*2*, *4*, *8*).

A typical visual prosthesis system would consist of a camera that the user wears on a pair of glasses and a portable processor that transforms camera footage into instructions for electrical stimulation of the visual cortex (*21*). We hypothesized that simultaneous stimulation of multiple electrodes would create recognizable shapes in the user's perception. The generation of artificial percepts would require a substantial number of functional electrodes in the visual cortex, covering a sufficiently large fraction of the visual field. Most previous studies have focused on the properties of individual phosphenes and the electrical stimulation parameters that reliably evoke them. One recent study (*22*) demonstrated shape perception by sequentially stimulating a number of electrodes positioned on the surface of the visual cortex, to trace out a shape. However, sequential stimulation limits the amount of information that can be transferred per unit of time, and the generation of shapes via simultaneous electrical stimulation of multiple electrodes in the visual cortex remains to be demonstrated (*23*, *24*).

An implant with 1024 electrodes in the visual cortex

Most [although not all (*3*, *8*)] previous studies in humans used electrodes that were positioned on the surface of the brain and required delivery of currents in the milliampere range, limiting the number of electrodes that could safely be stimulated at the same time. Surface electrodes activate several millimeters of cortex and produce large phosphenes, and this results in low spatial resolution. Furthermore, previous studies have observed interference between the percepts elicited by simultaneous stimulation on nearby electrodes (*2*, *3*, *11*, *22*). By contrast, microstimulation by intracortical electrodes requires currents that are two orders of magnitude lower (*3*, *8*, *15*, *16*, *19*), activates neurons located within a few hundred micrometers of the electrode tip, and potentially yields higher-resolution phosphene percepts (*25*) (supplementary text).

To investigate the generation of artificial visual percepts using a large number of intracortical electrodes, we created a 1024-channel implant consisting of a titanium pedestal connected to 16 Utah arrays (*26*), each with eight rows and columns of 1.5-mm-long shanks (fig. S1A). We tested the system in two macaque monkeys, L and A. In both monkeys, 14 arrays were tiled across the left primary visual cortex (area V1) (Fig. 1, A and B). Two arrays were placed in V4 (fig. S2), allowing us to monitor the effects of V1 stimulation on neuronal activity in a higher cortical area.

We presented moving bars (*27*) and obtained multiunit receptive fields (RFs) on 820 of 896 and 616 of 896 V1 electrodes and on 120 of 128 and 92 of 128 V4 electrodes in monkeys L and A, respectively (movies S1 and S2). In accordance with known retinotopy (*28*), the RFs covered the foveal and parafoveal regions of the lower right visual field, with V1 RF eccentricities of ≤9° and ≤5° (Fig. 1, C and D) and V4 RF eccentricities of ≤5° and ≤15° in monkeys L and A, respectively (fig. S2).

Saccade-to-phosphene task

We used a saccade-to-phosphene task (Fig. 2A and movie S3) to investigate phosphene locations and determine current thresholds for phosphene perception (N = 184 electrodes in monkey L, and N = 164 in monkey A). The monkeys had previously been trained to make eye movements to visually presented dots on a computer monitor, and we replaced the visual stimuli by electrical microstimulation on individual V1 electrodes. Figure 2B shows the probability of saccade execution as a function of current amplitude during stimulation of an example V1 electrode in monkey L. The current threshold, C_{50}, defined as the level at which the monkey reported the phosphene 50% of the time, was 12.6 μA. Across electrodes, the median threshold in monkey L was 23 μA [interquartile range (IQR), 6 to 40 μA] and in monkey A it was 50 μA (IQR, 43 to 58 μA) (Fig. 2C).

We recorded neuronal activity in V4 during V1 microstimulation (Fig. 2D) and removed the electrical artifacts caused by stimulation from the V4 signal (*28*). Figure 2E shows the mean response across 17 V4 electrodes, during the same session as that in Fig. 2B. The V4 activity increased as a function of V1 current amplitude, with a particularly steep relationship around the C_{50} of the electrode (Fig. 2F). We calculated the neurometric threshold, R_{50}, as the current amplitude at which V4 activity reached 50% of its maximum. The R_{50} was 12.4 μA, similar to the C_{50} of 12.6 μA. Across the currents tested on this V1 electrode, the correlation between the V4 activity level and hit rate was significant [correlation coefficient (r) = 0.94, $p < 0.001$ (Pearson's correlation)].

It would be advantageous if V4 activity could be used more generally to estimate V1 current thresholds, because prospective prosthesis users might experience fatigue during the determination of thresholds on hundreds of electrodes based on visibility reports. The R_{50} could be measured while the user is engaged in an unrelated activity. We observed a high correlation between the R_{50} and C_{50} in both animals [monkey L: r = 0.98, N = 169, $p < 0.001$, 104 unique V1 electrodes for which stimulation artifacts were removed successfully; monkey A: r = 0.96, N = 64, $p < 0.001$, 44 V1

[1]Department of Vision & Cognition, Netherlands Institute for Neuroscience, Meibergdreef 47, 1105 BA Amsterdam, Netherlands. [2]Bioengineering Institute and CIBER-BBN, Miguel Hernández University of Elche, Elche, Spain. [3]Department of Integrative Neurophysiology, VU University, De Boelelaan 1085, 1081 HV Amsterdam, Netherlands. [4]Department of Psychiatry, Academic Medical Centre, Postbus 22660, 1100 DD Amsterdam, Netherlands.
*Corresponding author. Email: x.chen@nin.knaw.nl (X.C.); p.roelfsema@nin.knaw.nl (P.R.R.)

electrodes (Pearson's correlation)] (Fig. 2G). To further test how well V4 activity relates to phosphene visibility, we divided the V1 electrodes into three equally large groups based on the C_{50} and determined the average V4 response as a function of V1 current amplitude within each group (Fig. 2H). The shape of V4 response as a function of current amplitude resembled the psychometric function within each group, confirming that V4 activity can be used to estimate V1 current thresholds.

Although we used a large target window (see methods), the monkeys' eye movements were generally directed toward the RFs of the stimulated neurons (*14*) (compare Fig. 1, E and F to C and D; movie S3). To quantify this relationship, we computed the correlation between the polar angle of the mean saccadic end point and that of the RF (Fig. 2, I and J), which was significant in both monkeys (monkey L: $r = 0.77$, $p < 0.001$, $N = 184$; monkey A: $r = 0.67$, $p < 0.001$, $N = 164$). The correlation between the eccentricity of the saccade end point and that of the RF was also significant [monkey L: $r = 0.90$, $p < 0.001$; monkey A, $r = 0.72$, $p < 0.001$ (Pearson's correlation)], although there was a consistent undershoot of the saccade relative to the RF [saccade amplitude as a fraction of RF eccentricity in monkey L: 0.77 ± 0.18 (mean ± SD), $N = 184$; monkey A: 0.71 ± 0.21, $N = 164$], which was more pronounced for weaker stimulation currents (fig. S3). These findings confirm that phosphenes are perceived at the RF of the stimulated neurons (*9*, *10*, *12*, *14*, *17*, *20*). The next experiments addressed whether multielectrode stimulation elicits interpretable artificial percepts.

Generation of composite visual percepts

First, we tested whether the monkeys could report the spatial alignment of two phosphenes (vertical or horizontal) by requiring them to saccade to a target above or below the fixation spot, respectively (Fig. 3A and movie S4). Before array implantation, the animals were trained extensively on a visual version of the task, in which they reported the relative position of two small dots on a screen. In every session of the microstimulation task, we selected unfamiliar pairs of electrodes for simultaneous stimulation, such that the RFs of the stimulated neurons were vertically or horizontally aligned.

Figure 3B shows the results for an example session, with mean accuracies of 91 and 88% for the vertical and horizontal conditions, respectively. Performance was above chance level from the start of the session even though the electrode set was novel, which suggests that the monkey generalized its understanding from the visual to the phosphene version of the task. The average accuracy across sessions with novel electrode pairs was significantly above chance [monkey L: 70 ± 13%, $N = 19$ electrode sets, $t_{18} = 6.6$, $p < 0.001$; monkey A: 64 ± 18%, $N = 11$, $t_{10} = 2.6$, $p = 0.026$ (one-sample t test)] (Fig. 3C). We also ran a visual version of the task in which we presented dots on the screen at the RF locations. Monkey L reached an accuracy of 83 ± 10% ($t_{18} = 15$, $p < 0.001$), and monkey A 79 ± 15% ($t_{10} = 6.2$, $p < 0.001$). These visually presented dot configurations were not always novel, that is, the monkeys had seen some of these dot pairs in previous sessions.

We rewarded the monkeys after correct saccades; hence, they might have learned to associate arbitrary phosphene percepts with specific targets by trial and error. We therefore computed the mean accuracy across electrode sets during the first 30 trials of the microstimulation task (Fig. 3D). The animals' accuracies remained relatively stable across time. For both monkeys, we determined the critical trial, c, for which the accuracy was higher than chance ($p < 0.05$, binomial test) when trials 1 through c were included, across electrode sets (*28*). In monkey L, c was the first trial [responses were correct on 17 of 19 electrode sets; $p < 0.001$ (binomial test)], and in monkey A, c was the fourth trial (30 of 44 electrode sets and trials; $p = 0.011$). Furthermore, no significant improvement in performance occurred between trials 1 to 10 and trials 21 to 30 [monkey L: $t_{18} = 0.0$, $p = 1.0$; monkey A: $t_{10} = 0.17$, $p = 0.87$ (paired t test)]. We conclude that the monkeys generalized from their experience on the visual task to judge whether novel phosphene pairs were horizontally or vertically aligned.

Direction-of-motion task

The monkeys had also been trained to report the apparent motion direction of a sequence of visually presented dots. We investigated whether the monkeys could interpret the direction of successively generated phosphenes (Fig. 3E and movie S5). We selected three electrodes with a vertical or horizontal offset and stimulated them sequentially such that their RFs formed a sequence, going from top to bottom or bottom

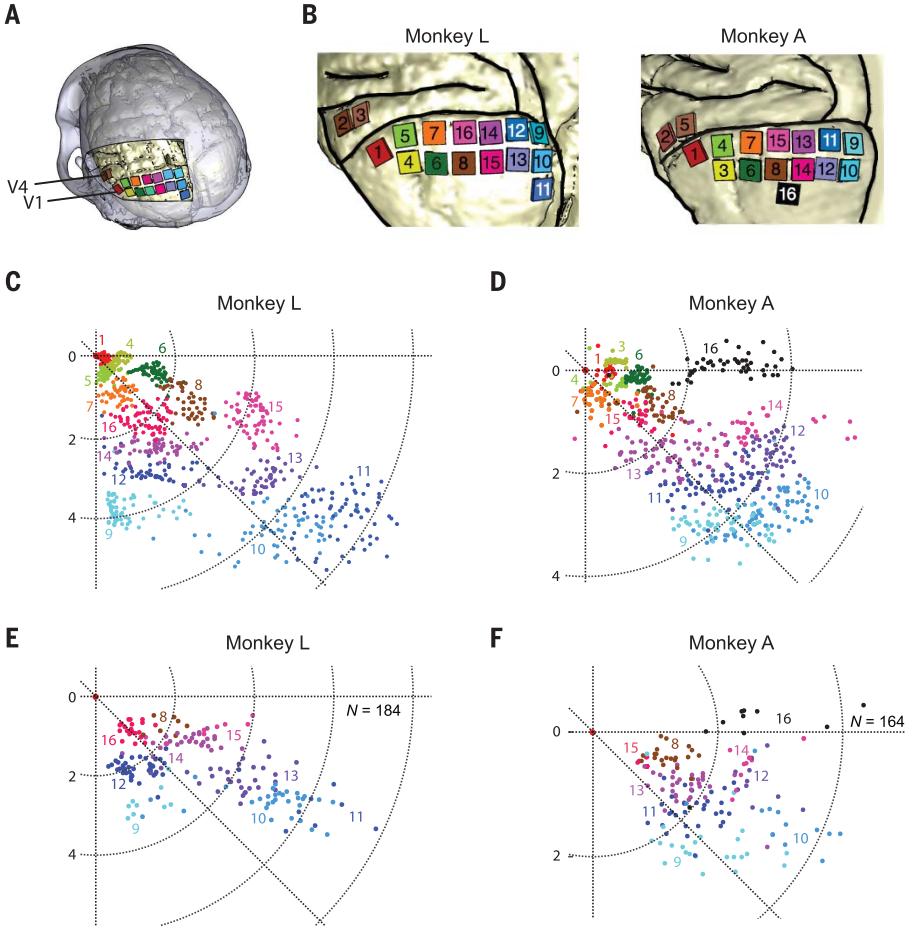

Fig. 1. Location of electrodes and receptive fields. (**A**) Locations of arrays in areas V1 and V4 of the visual cortex in the left hemisphere of monkey L. (**B**) Higher-magnification view of array locations. Array numbers correspond to the order of attachment between the arrays and the pedestal. (**C** and **D**) RF centers. Colors correspond to those of the arrays in (A) and (B). (**E** and **F**) Average saccadic end points. Colors correspond to those of the arrays in (A) and (B).

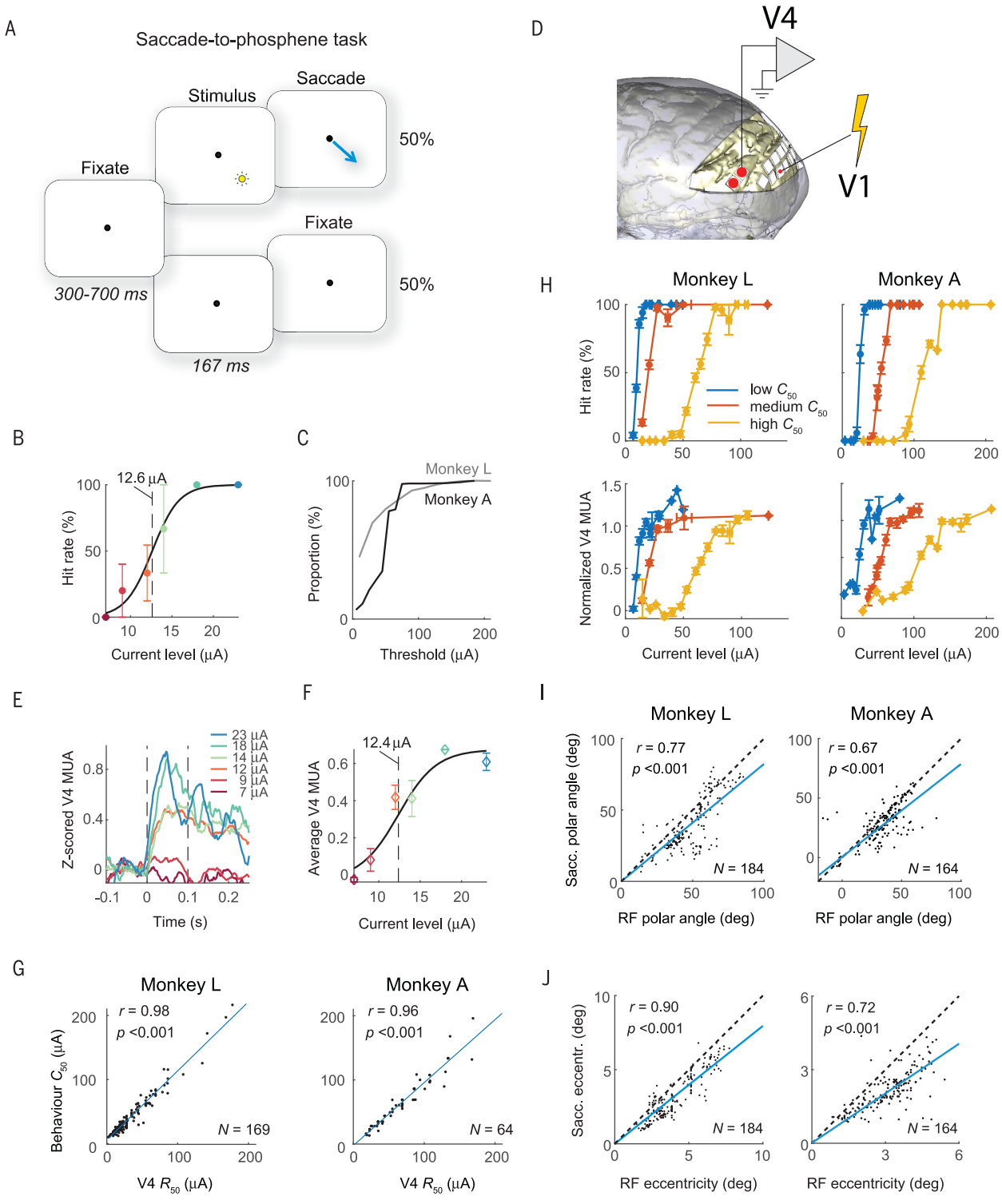

Fig. 2. Saccade-to-phosphene task. (**A**) Illustration of the task. The yellow circle represents a phosphene; the arrow represents an eye movement to the artificially induced perception. (**B**) Probability of eliciting a saccade, as a function of current amplitude, during stimulation on an example V1 electrode in monkey L. The dashed line indicates the current threshold; error bars represent SEM. (**C**) Cumulative distribution of current thresholds. (**D**) Schematic showing recording from V4 during V1 microstimulation. (**E**) Time course of activity (relative to stimulation onset), averaged across V4 channels during V1 microstimulation [same session as in (B)]. The dashed lines indicate the time window during which V4 activity was measured. (**F**) V4 activity as a function of stimulation current [same session as in (B) and (E)]. The dashed line indicates the current threshold; error bars represent SEM. (**G**) Correlation between current thresholds derived from neurometric (R_{50}) and psychometric functions (C_{50}). (**H**) Mean performance (top) and mean V4 response (bottom) as a function of current amplitude for V1 electrodes with low (blue), intermediate (red), and high thresholds (yellow; tertiles). Vertical error bars represent SEM of performance levels (upper) or V4 responses (lower); horizontal error bars represent SEM of current levels. (**I** and **J**) Comparison of polar angle (I) and eccentricity (J) between RFs and saccadic end points. The blue line shows a linear regression, which was constrained to pass through the origin.

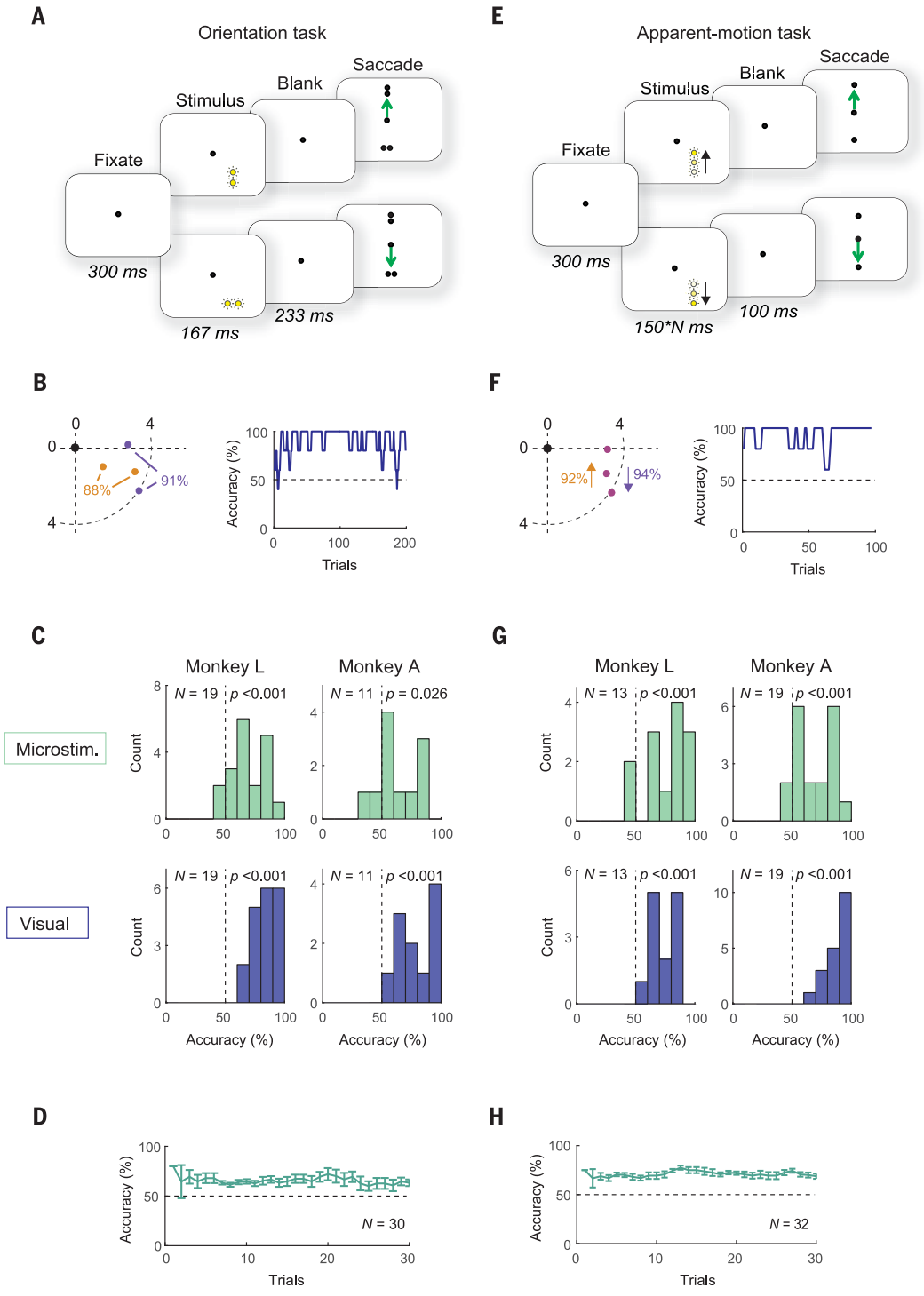

Fig. 3. Two-phosphene orientation and direction of motion task. (**A**) Two-phosphene orientation discrimination task. The monkey reported with an eye movement whether two phosphenes (or visually presented dots) were oriented horizontally or vertically. (**B**) (Left) RF centers for an example set of four electrodes in monkey A. Black circle, fixation point; orange dots, horizontal condition; purple dots, vertical condition. (Right) Accuracy (averaged across five trials) for this example set. (**C**) Distribution of accuracies across electrode sets during microstimulation (green) and visual (blue) versions of the task. (**D**) Mean accuracy across electrode sets and monkeys, as a function of trial number, on the microstimulation version of the task (averages and SEM across five trials). (**E**) Direction-of-motion task. (**F**) (Left) RF centers for an example set of three electrodes, stimulated in sequence (indicated by arrows). (Right) Accuracy for this example set. (**G** and **H**) Similar to (C) and (D), for the direction-of-motion task.

to top for "vertical" sets of electrodes and left to right or right to left for "horizontal" sets of electrodes. Figure 3F illustrates an example session in monkey A, in which the RFs had a vertical offset and the monkey reached high accuracy from the first trial onward. Across all electrode sets of the microstimulation task (Fig. 3G), the average accuracies of monkeys L and A were 76 ± 17% [$N = 13$, $t_{12} = 5.5$, $p < 0.001$ (t test)] and 69 ± 16% ($N = 19$, $t_{18} = 5.2$, $p < 0.001$), respectively. The monkeys' accuracies for novel electrode combinations were higher than chance from the first trials onward. The critical trial c was trial 1 in monkey L (correct on the first trial in 11 of 13 sessions; $p = 0.011$) and trial 4 in monkey A (trials 1 to 4, 48 of 76 correct; $p = 0.014$) (Fig. 3H), indicating that they were able to generalize their understanding of apparent motion from the visual to the phosphene task. No significant improvement in performance occurred between trials 1 to 10 and trials 21 to 30 [monkey L: $t_{12} = 1.35$, $p = 0.2$; monkey A: $t_{18} = -1.85$, $p = 0.08$ (paired t test)]. The accuracies of monkeys L and A in the task with a sequence of visually presented dots were 74 ± 11% ($t_{12} = 8.2$, $p < 0.001$) and 89 ± 11% ($t_{18} = 15.6$, $p < 0.001$), respectively, although these dot combinations were not always novel.

Letter task

Next, we examined the possibility of creating more complex shape percepts. We delivered

stimulation on 8, 10, or 15 electrodes in V1 simultaneously, selecting the electrode sets such that the RFs collectively formed the shape of one of two letters. The number of stimulated electrodes was always the same between the two conditions in a given session. Before electrode implantation, the monkeys had learned to report the identity of 16 visually presented letters on a screen by making an eye movement to a target. The training program also included letters presented as sparse dot patterns, designed to simulate phosphene vision (fig. S4) (*29*). After array implantation, the training continued, and we initially alternated visual and microstimulation blocks. Thereafter, sessions consisted solely of visual or microstimulation trials. During visual trials, one of two letters was presented as a dot pattern on the screen. During microstimulation trials, we delivered simultaneous electrical stimulation to a novel set of electrodes for 167 ms (50 pulses at 300 Hz) (Fig. 4A and movie S6).

Figure 4B shows the accuracy of monkey A for an example set of electrodes on the microstimulation version of the task. In one condition, the RFs of the stimulated electrodes formed the letter T (orange dots) and in the other condition they formed the letter L (purple dots). In this example session, accuracy was 0.89 and 0.96 for the T and L conditions, respectively, and it was relatively high from the first trial onward. Across all electrode sets (Fig. 4C), the average accuracy of monkey L was 81 ± 18% [$N = 9$, $t_8 = 5.4$, $p < 0.001$ (t test)] and the accuracy of monkey A was 71 ± 18% ($N = 10$, $t_9 = 3.6$, $p = 0.006$) on the microstimulation version of the task. Accuracy on the visual version of the task was 88 ± 5% for monkey L ($t_8 = 23.1$, $p < 0.001$) and 93 ± 4% for monkey A ($t_9 = 36.7$, $p < 0.001$), although some of these dot displays were not novel.

To control for the possibility that the monkeys learned to map arbitrary percepts onto saccade targets, we examined the accuracy time course (Fig. 4D). The critical trial c (accuracy above chance level, binomial test) was trial 3 in monkey L (20 of 27 correct, $p = 0.0096$), and trial 7 in monkey A (43 of 70 correct, $p = 0.036$). No significant improvement in performance occurred between trials 1 to 10 and trials 21 to 30 [monkey L: $t_8 = -0.7$, $p = 0.5$; monkey A: $t_9 = 0.7$, $p = 0.5$ (paired t test)].

As a further control, we examined how long it took the monkeys to associate arbitrary microstimulation patterns with eye movements. We selected novel, nonoverlapping combinations of electrodes, such that their RFs did not form any recognizable letter ($N = 10$ electrode sets in both monkeys). The mean accuracy of monkeys L and A during the first 100 trials was close to chance level (48.2 and 46.9%; $p > 0.2$ in both monkeys) (gray data points in Fig. 4D) and lower than during the first 100 trials of the microstimulation task with familiar letters (monkey L, $t_{17} = 5.7$, $p < 0.001$; monkey A, $t_{18} = 2.4$, $p = 0.03$). We also ran a visual version of the control task, in which the monkeys saw two novel visual dot stimuli. The mean accuracies of monkeys L and A were 50.5 and 49.9%, respectively ($p > 0.9$), indicating that they also failed to rapidly learn to map unfamiliar dot stimuli onto saccade targets (Fig. 4D and fig. S5).

These results indicate that the monkeys' abilities to perform the letter task were not due to rapid learning of new associations between stimuli and eye movement targets. Rather, the phosphene percepts must have borne a close resemblance to the visually presented letters, allowing the monkeys to benefit from their extensive prior experience.

Discussion

We demonstrated that the simultaneous stimulation of multiple electrodes in V1 gives rise to the perception of shape and that successive stimulation gives rise to the perception of motion, providing proof of concept for the use of electrical microstimulation to create a form of artificial vision in the blind. Previous studies suggested that the successful generation of phosphene percepts can be read out in higher visual cortical areas (*30*, *31*). Here, we demonstrated how V4 activity can be used to determine phosphene thresholds in V1, circumventing a time-consuming calibration process in which the prosthesis user has to report whether currents are above or below the perceptual threshold on hundreds of electrodes.

These results capitalized on several developments. First, we implanted a large number of electrodes with foveal and parafoveal coverage of one quadrant of the visual field. Simulations of phosphene vision estimated that whereas letter recognition is possible with a few hundred electrodes, fluent reading and object recognition in crowded scenes may require thousands of electrodes (*32*, *33*). By implanting more than 1000 electrodes across a large area of V1, we could generate numerous phosphenes across a contiguous region of the visual field (Fig. 1) and elicit recognizable shapes (Figs. 3 and 4).

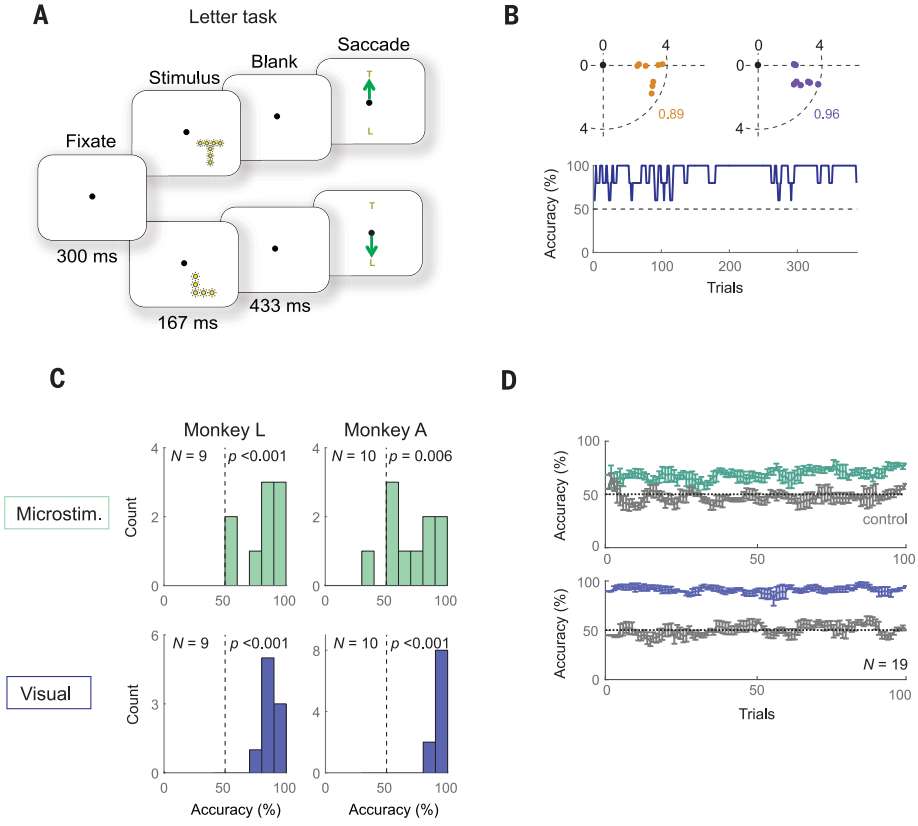

Fig. 4. Letter recognition task. (**A**) Illustration of the task. The monkey reported letter identity with an eye movement. (**B**) (Top) RF centers of eight stimulated V1 electrodes whose RF centers formed a T or an L (orange and purple circles). (Bottom) Accuracy (smoothed across five trials) for this example set. (**C**) Accuracy for sessions on microstimulation (green) and visual (blue) versions of the task. (**D**) Mean accuracy across electrode sets and monkeys, as a function of trial number (average and SEM across five trials) in the microstimulation (green) and visual (blue) versions of the task. In a control task with novel electrical stimulation and visually presented dot patterns, the accuracy was close to chance (gray).

Secondly, we used intracortical electrodes, which have advantages over the subdural electrodes used in previous human studies (*2*, *10*, *34*). Subdural electrodes require currents in the milliampere range and activate populations of neurons across millimeters of cortex (*9*, *10*), which limits their resolution. Furthermore, the stimulation of adjacent subdural electrodes may cause interference, generating a single, large phosphene instead of several small ones. Using depth electrodes, we elicited phosphenes with median stimulation currents of 23 to 50 μA, which activate small populations of neurons located within a few hundred micrometers of the electrode tip (*25*). Hence, intracortical electrodes induce smaller and more precise phosphene percepts (*3*, *8*), but a systematic comparison of phosphenes produced by subdural and intracortical stimulation has yet to be performed (supplementary text) (*24*).

Third, before implantation the monkeys underwent intensive training on visual versions of the tasks, in which they saw shapes composed of small dots, designed to simulate phosphene percepts (*29*). As a result, the monkeys were immediately able to correctly interpret shape and motion stimuli composed of multiple phosphenes. Nevertheless, the monkeys made mistakes and even performed close to chance for several electrode sets. The accuracy in the tasks with visually presented dot patterns was also not perfect, indicating that the monkeys did not always recognize them, although this may have been caused by occasional drops in motivation (e.g., at the end of a recording session). We expected the accuracy for the tasks with electrical stimulation to be worse, because it is not possible to control the appearance of individual phosphenes. Humans report that phosphenes induced by stimulation of early visual cortical areas vary in color, brightness, shape, and perceived distance (*3*, *6*, *8*, *35*). Furthermore, simultaneous stimulation on two electrodes that are a few hundred micrometers apart can yield fused phosphenes (*3*). Such variability and potential interactions may make electrically induced percepts more difficult to interpret than visually presented ones.

A number of technical hurdles still have to be overcome before a visual cortical prosthesis is available for humans. The mean surface area of human primary visual cortex is 25 to 30 cm^2 per hemisphere, and future implants should cover a large enough region of the visual field with a sufficient density of phosphenes to generate interpretable percepts (*36*, *37*). Furthermore, it will be necessary to create wireless technology with high channel counts and to develop long-lasting, biocompatible electrodes that minimize the risk of gliosis, tissue trauma, and encapsulation (*38*). Much progress is being made in the development of brain-computer interfaces for sensory restoration and motor prostheses (*39*–*41*). Combined with the present demonstration of artificial vision, these developments place a light at the end of the tunnel for those without sight.

REFERENCES AND NOTES

1. W. H. Dobelle, M. G. Mladejovsky, J. P. Girvin, *Science* **183**, 440–444 (1974).
2. J. Button, T. Putnam, *J. Iowa Med. Soc.* **52**, 17 (1962).
3. G. S. Brindley, W. S. Lewin, *J. Physiol.* **196**, 479–493 (1968).
4. M. Bak *et al*., *Med. Biol. Eng. Comput.* **28**, 257–259 (1990).
5. W. H. Dobelle, M. G. Mladejovsky, J. R. Evans, T. S. Roberts, J. P. Girvin, *Nature* **259**, 111–112 (1976).
6. J. R. Evans, J. Gordon, I. Abramov, M. G. Mladejovsky, W. H. Dobelle, *Sens. Processes* **3**, 82–94 (1979).
7. D. N. Rushton, G. S. Brindley, in *Physiological Aspects of Clinical Neurology*, F. C. Rose, Ed. (Blackwell Scientific Publications, ed. 1, 1977), pp. 123–153.
8. E. M. Schmidt *et al*., *Brain* **119**, 507–522 (1996).
9. J. Winawer, J. Parvizi, *Neuron* **92**, 1213–1219 (2016).
10. W. H. Bosking *et al*., *J. Neurosci.* **37**, 7188–7197 (2017).
11. J. R. Bartlett *et al*., *J. Neurophysiol.* **94**, 3430–3442 (2005).
12. D. C. Bradley *et al*., *J. Neurophysiol.* **93**, 1659–1670 (2005).
13. E. A. DeYoe, J. D. Lewine, R. W. Doty, *J. Neurophysiol.* **94**, 3443–3450 (2005).
14. T. S. Davis *et al*., *J. Neural Eng.* **9**, 065003 (2012).
15. B. Dagnino, M. A. Gariel-Mathis, P. R. Roelfsema, *J. Neurophysiol.* **113**, 730–739 (2015).
16. D. K. Murphey, J. H. R. Maunsell, *Curr. Biol.* **17**, 862–867 (2007).
17. E. J. Tehovnik, W. M. Slocum, P. H. Schiller, *Eur. J. Neurosci.* **17**, 870–878 (2003).
18. E. J. Tehovnik, W. M. Slocum, *Eur. J. Neurosci.* **29**, 1477–1489 (2009).
19. K. Torab *et al*., *J. Neural Eng.* **8**, 035001 (2011).
20. P. Troyk *et al*., *Artif. Organs* **27**, 1005–1015 (2003).
21. P. M. Lewis, J. V. Rosenfeld, *Brain Res.* **1630**, 208–224 (2016).
22. M. S. Beauchamp *et al*., *Cell* **181**, 774–783.e5 (2020).
23. W. H. Bosking, M. S. Beauchamp, D. Yoshor, *Annu. Rev. Vis. Sci.* **3**, 141–166 (2017).
24. A. N. Foroushani, C. C. Pack, M. Sawan, *J. Neural Eng.* **15**, 021005 (2018).
25. M. H. Histed, V. Bonin, R. C. Reid, *Neuron* **63**, 508–522 (2009).
26. P. J. Rousche, R. A. Normann, *J. Neurosci. Methods* **82**, 1–15 (1998).
27. Materials and methods are available as supplementary materials.
28. R. B. Tootell, E. Switkes, M. S. Silverman, S. L. Hamilton, *J. Neurosci.* **8**, 1531–1568 (1988).
29. N. J. Killian, M. Vurro, S. B. Keith, M. J. Kyada, J. S. Pezaris, *Sci. Rep.* **6**, 36329 (2016).
30. M. S. Beauchamp, P. Sun, S. H. Baum, A. S. Tolias, D. Yoshor, *Nat. Neurosci.* **15**, 957–959 (2012).
31. B. van Vugt *et al*., *Science* **360**, 537–542 (2018).
32. B. Bourkiza, M. Vurro, A. Jeffries, J. S. Pezaris, *PLOS ONE* **8**, e73592 (2013).
33. J.-H. Jung, D. Aloni, Y. Yitzhaky, E. Peli, *Vision Res.* **111**, 182–196 (2015).
34. W. H. Dobelle, M. G. Mladejovsky, *J. Physiol.* **243**, 553–576 (1974).
35. P. H. Schiller, W. M. Slocum, M. C. Kwak, G. L. Kendall, E. J. Tehovnik, *Proc. Natl. Acad. Sci. U.S.A.* **108**, 17809–17814 (2011).
36. L. E. Hallum, G. Dagnelie, G. J. Suaning, N. H. Lovell, *J. Neural Eng.* **4**, S58–S71 (2007).
37. S. C. Chen, G. J. Suaning, J. W. Morley, N. H. Lovell, *Vision Res.* **49**, 2329–2343 (2009).
38. L. Luan *et al*., *Sci. Adv.* **3**, e1601966 (2017).
39. P. R. Roelfsema, D. Denys, P. C. Klink, *Trends Cogn. Sci.* **22**, 598–610 (2018).
40. S. N. Flesher *et al*., *Sci. Transl. Med.* **8**, 361ra141 (2016).
41. L. R. Hochberg *et al*., *Nature* **485**, 372 (2012).
42. X. Chen, F. Wang, E. Fernandez, P. Roelfsema, Data repository for "Shape perception via a high-channel-count neuroprosthesis in monkey visual cortex," Version 1, Mendeley Data (2020); https://doi.org/10.17632/gx39r48w3b.1.

ACKNOWLEDGMENTS

We thank K. Brandsma, A. Ditewig, and L. Beekman for biotechnical support; M. Self and R. Schuurman for assistance during surgeries; and B. Li, R. van Wezel, J.-A. Sahel, S. Picaud, R. Goebel, M. Self, and G. Dagnelie for feedback on the manuscript. We thank F. Solzbacher, M. Gerhardt, R. Franklin, N. Halper, S. Hou, K. Torab, and others at Blackrock Microsystems for assistance. **Funding:** The work was supported by NWO (STW-Perspectief P15-42 "NESTOR"), the European Union FP7 (ERC 339490 "Cortic_al_gorithms"), the Human Brain Project (agreements 720270 and 785907, "Human Brain Project SGA1 and SGA2"), and the Friends Foundation of the Netherlands Institute for Neuroscience. **Author contributions:** X.C. and P.R.R. designed the study with input from E.F.; X.C. ran the experiments and collected the data; X.C. and F.W. analyzed the data; X.C., P.R.R., and F.W. wrote the manuscript with advice from E.F.; and P.R.R. supervised the project. **Competing interests:** P.R.R. and X.C. are cofounders and shareholders of a neurotechnology start-up, Phosphoenix (Netherlands). P.R.R. and X.C. registered a patent related to this work, WO2020043790 (A1). **Data and materials availability:** The data and the computer code used to analyze the data are available for download from Mendeley Data (*42*).

SUPPLEMENTARY MATERIALS

science.sciencemag.org/content/370/6521/1191/suppl/DC1
Materials and Methods
Supplementary Text
Figs. S1 to S6
References (*43*–*56*)
MDAR Reproducibility Checklist
Movies S1 to S6

View/request a protocol for this paper from *Bio-protocol*.

14 July 2020; accepted 19 October 2020
10.1126/science.abd7435

Science

Shape perception via a high-channel-count neuroprosthesis in monkey visual cortex

Xing Chen, Feng Wang, Eduardo Fernandez and Pieter R. Roelfsema

Science **370** (6521), 1191-1196.
DOI: 10.1126/science.abd7435

Restoring vision by stimulating the brain

Electrical stimulation of the visual cortex has long been proposed as an approach to restoring vision in blind people. Previous studies positioned electrodes on the surface of the brain and thus required delivery of relatively high currents. However, this approach limits the number of electrodes that can be safely stimulated simultaneously, and such surface electrodes activate several millimeters of cortex, which results in a low spatial resolution. Chen *et al.* demonstrated that the simultaneous stimulation of multiple intracortical electrodes in the monkey primary visual cortex gives rise to the perception of shape and successive stimulation to the perception of motion (see the Perspective by Beauchamp and Yoshor). This major improvement provides proof of concept for the use of electrical microstimulation to create a form of artificial vision in the blind.

Science, this issue p. 1191; see also p. 1165

Science (print ISSN 0036-8075; online ISSN 1095-9203) is published by the American Association for the Advancement of Science, 1200 New York Avenue NW, Washington, DC 20005. The title *Science* is a registered trademark of AAAS.